

Interpretable, predictive spatio-temporal models via enhanced Pairwise Directions Estimation

Heng-Hui Lue

Department of Statistics,
Tunghai University
Taichung, Taiwan
hhlue@thu.edu.tw

ShengLi Tzeng

Department of Applied Mathematics,
National Sun Yat-sen University,
Kaohsiung, Taiwan
slt.cmu@gmail.com

Summary

This article concerns the predictive modeling for spatio-temporal data as well as model interpretation using data information in space and time. Intrinsically, we develop a novel approach based on dimension reduction for such data in order to capture nonlinear mean structures without requiring a prespecified parametric model. In addition to prediction as a common interest, this approach focuses more on the exploration of geometric information in the data. The method of Pairwise Directions Estimation (PDE) is incorporated in our approach to implement the data-driven function searching of spatial structures and temporal patterns, useful in exploring data trends. The benefit of using geometrical information from the method of PDE is highlighted. We further enhance PDE, referring to it as PDE+, by using resolution adaptive fixed rank kriging to estimate the random effects not explained in the mean structures. Our proposal can not only produce more accurate and explainable prediction, but also increase the computation efficiency for model building. Several simulation examples are conducted and comparisons are made with four existing methods. The results demonstrate that the proposed PDE+ method is very useful for exploring and interpreting the patterns of trend for spatio-temporal data. Illustrative applications to two real datasets are also presented.

KEYWORDS

covariates, dimension reduction, kriging, semi-parametric models, visualization

1 Introduction

Spatio-temporal phenomena are often complicated, but kriging methods are widely used in modeling such data, where only a very simple mean structure is assumed. There are two components in typical kriging; namely, a stationary Gaussian process plus a mean function. Most of kriging approaches take either some “known” functional forms of covariates in the mean function (universal kriging), or even a constant as the global mean (ordinary kriging).

Martin and Simpson (2005) showed that ordinary kriging can have poor prediction under the presence of strong trends. To explore the important spatial structure for spatio-temporal data, the empirical orthogonal function (EOF) analysis is a commonly

used method, which is based on principal component analysis approach; see Cressie and Wikle (2011) and Demsar et al. (2013) for review. EOFs usually provide the meaningful bases for spatial or spatio-temporal random-effects representation, e.g., Braud and Obled (1991) and Thorson et al. (2020). However, EOF analysis treats data at n locations as random variables and observations at T time points as independent samples, and hence that will cause EOFs to be problematic if $n > T$. Wang and Huang (2017) proposed a regularized method to find the smooth and localized dominant spatial patterns to overcome the limitation of $n > T$ issue.

In the terminology of kriging, EOFs and their modified versions mainly focus on the stochastic process part. Very few tools are available for modeling strong patterns in the mean function, even if several methods for large-scale spatial or spatio-temporal prediction were proposed in the past decade (e.g., Cressie and Johannesso, 2008; Fassò and Cameletti, 2010; Cressie et al. 2010; Ma and Kang, 2020).

In this article, we focus on the reduction of dimension for specific spatio-temporal outcomes in order to detect important spatial structures and temporal patterns in the mean trend of such data. We shall propose a novel approach to adaptively capture potentially complicated mean structures with a not-always-stationary Gaussian process. Despite recent flourish of research on dimension reduction, such time relevant high-dimensional data remains to be challenging (e.g., Li, et al. (2003), Lue, 2019; Coudret et al. 2014).

In addition to the parametric form of covariates as in the universal kriging, we also introduce a superposition from the inner products of nonparametric spatial structures and nonparametric temporal functions. As shown in the application to two real datasets of Section 4, these extra inner products aid in exploring and interpreting how the spatio-temporal patterns vary with location and/or with time. Those findings can formulate new hypotheses or link the phenomena to some documented but imperceptible knowledge.

Though EOFs analysis are exploratory and explanatory, they usually come into prediction in a two-stage manner, namely reconstructing the covariance function followed by another model for prediction. In contrast, our proposed method simultaneously gives the explainable spatial structures and temporal patterns, as well as a predictive model. Our proposal not only can capture more sophisticated mean structures, but may also produce more accurate prediction. Moreover, the computation efficiency can be easily recognized.

The remainder of the paper is organized as follows. Section 2 introduces our approach. We use three simulation examples to illustrate and evaluate our proposed method in Section 3. Section 4 applies our method to two real datasets, and Section 5 concludes with discussion on future work.

2 Proposed Method

Consider a sequence of spatial processes, $\{z(\mathbf{s}, t) : \mathbf{s} \in \mathcal{D}\}$ for $t = 1, \dots, T$, defined on a d -dimensional spatial domain $\mathcal{D} \subset \mathbb{R}^d$ with $T \geq 1$. The processes are assumed to have a common spatial covariance function $C(\mathbf{s}, \mathbf{s}^*) = \text{cov}(z(\mathbf{s}, t), z(\mathbf{s}^*, t))$ invariant over time and a mean function in a form of

$$\mu(\mathbf{s}, t) = \sum_{i=1}^Q \alpha_i \zeta_i(\mathbf{s}, t) + \sum_{j=1}^{\kappa} w_j(t) \tilde{f}_j(\mathbf{s}), \quad (1)$$

where $\zeta_i(\mathbf{s}, t)$'s are observed spatio-temporal covariates varying with locations \mathbf{s} and time t , α_i 's are unknown parameters, $w_j(t)$ is an unknown basis function changing smoothly with time t , and $\tilde{f}_j(\mathbf{s})$ is an unknown coefficient function standing for a certain spatial

pattern. We further assume that the function $\tilde{f}_j(\mathbf{s})$ can be formulated as $f_j(\boldsymbol{\theta}'_j \mathbf{x}(\mathbf{s}))$ depending on a $P \times 1$ vector $\mathbf{x}(\mathbf{s})$ consisting of spatial-only covariates at location \mathbf{s} , and $\boldsymbol{\theta}_j$ is an unknown vector of weights. We refer to $\boldsymbol{\theta}'_j \mathbf{x}(\mathbf{s})$ as a variate. Hence, $\tilde{f}_j(\mathbf{s})$ can incorporate more covariates other than locations and determining $\tilde{f}_j(\mathbf{s})$ amounts to finding both f_j and $\boldsymbol{\theta}_j$, which is a typical theme in supervised dimension reduction via constructing new variate $\boldsymbol{\theta}'_j \mathbf{x}(\mathbf{s})$ instead of using $\mathbf{x}(\mathbf{s})$ directly.

The rationale for the second term of inner products in (1) comes from Taylor expansion. Consider a general function $g(s, t)$ with all the κ -th partial derivatives exist at a point (s_0, t_0) for $s, s_0 \in \mathfrak{R}$. Then the κ -th degree Taylor polynomial approximation of g for (s, t) near (s_0, t_0) is

$$g(s, t) \approx \sum_{i=1}^{\kappa} \sum_{j=1}^{\kappa-1} \frac{1}{i!j!} \cdot \frac{\partial^{(i+j)}}{\partial^i t \partial^j s} g(s_0, t_0) \cdot (t - t_0)^i \cdot (s - s_0)^j,$$

namely, summation over the scaled products of polynomial functions of t and polynomial functions of s . For $\mathbf{s}, \mathbf{s}_0 \in \mathfrak{R}^d$, the expansion is similar. Under some smoothness conditions, such sum-of-products expansion is quite flexible.

Here we use two kinds of covariate information. A simple example of spatio-temporal covariates is to set $Q = T$ and let $\{\zeta_i(\mathbf{s}, t) = \mathbb{I}(t = i); i = 1, \dots, T\}$, where \mathbb{I} is the indicator function. Such $\zeta_i(\mathbf{s}, t)$ is all the same over locations at a time t , and hence it can represent a temporal-only trend. For spatial-only covariates $\mathbf{x}(\mathbf{s})$ over \mathfrak{R}^d , the simplest one is $(s_1, \dots, s_d)'$ and so $P = d$. We also consider $(s_1, \dots, s_d, s_1^2, \dots, s_d^2)'$ in our simulation examples and real data applications. Of course, we can add more elaborate and domain-specific covariates into either $\zeta_i(\mathbf{s}, t)$ or $\mathbf{x}(\mathbf{s})$, which would be helpful to comprehend and to interpret the spatio-temporal phenomenon.

Suppose that we observe data $y(\mathbf{s}_i, t)$, $i = 1, \dots, n$; $t = 1, \dots, T$, at n distinct locations, $\mathbf{s}_1, \dots, \mathbf{s}_n \in \mathcal{D}$. The data can also be represented as a matrix \mathbf{Y} with the (i, t) element being $y(\mathbf{s}_i, t)$. Let $\mathbf{y}(\cdot, t) = (y(\mathbf{s}_1, t), \dots, y(\mathbf{s}_n, t))'$ and $\mathbf{y}(\mathbf{s}, \cdot) = (y(\mathbf{s}, 1), \dots, y(\mathbf{s}, T))'$. Define a $T \times \kappa$ matrix for taking values of basis functions at time points $t = 1, \dots, T$,

$$\mathbf{W} = \begin{bmatrix} w_1(1) & \cdots & w_\kappa(1) \\ \vdots & \ddots & \vdots \\ w_1(T) & \cdots & w_\kappa(T) \end{bmatrix} = (\mathbf{w}_1, \dots, \mathbf{w}_\kappa) = \begin{bmatrix} \mathbf{w}(1) \\ \vdots \\ \mathbf{w}(T) \end{bmatrix},$$

that is, $\mathbf{w}_j = (w_j(1), \dots, w_j(T))'$ is a $T \times 1$ column vector while $\mathbf{w}(t) = (w_1(t), \dots, w_\kappa(t))$ is a $1 \times \kappa$ row vector. The spatio-temporal random effects model of $y(\mathbf{s}, t)$ with a measurement error ε is considered as

$$y(\mathbf{s}, t) = z(\mathbf{s}, t) + \varepsilon(\mathbf{s}, t), \quad (2)$$

$$z(\mathbf{s}, t) = \boldsymbol{\alpha}' \boldsymbol{\zeta}(\mathbf{s}, t) + \mathbf{w}(t) \mathbf{f}(\mathbf{x}(\mathbf{s})) + u(\mathbf{s}, t), \quad (3)$$

for $t = 1, \dots, T$, where $\boldsymbol{\alpha} = (\alpha_1, \dots, \alpha_Q)'$, $\boldsymbol{\zeta}(\mathbf{s}, t) = (\zeta_1(\mathbf{s}, t), \dots, \zeta_Q(\mathbf{s}, t))'$, $\mathbf{f}(\mathbf{x}(\mathbf{s})) = (f_1(\boldsymbol{\theta}'_1 \mathbf{x}(\mathbf{s})), \dots, f_\kappa(\boldsymbol{\theta}'_\kappa \mathbf{x}(\mathbf{s})))'$, $u(\mathbf{s}, t)$ is a zero-mean random effect with a covariance function $C(\mathbf{s}, \mathbf{s}^*) = \text{cov}(u(\mathbf{s}, t), u(\mathbf{s}^*, t))$, and $\varepsilon(\mathbf{s}, t) \sim N(0, \sigma_\varepsilon^2(t))$ is an additive white-noise uncorrelated with $z(\mathbf{s}, t)$. We also assume that $u(\cdot, t)$ and $\varepsilon(\cdot, t)$ are mutually uncorrelated, and $u(\mathbf{s}, t)$ is also independent of $u(\mathbf{s}^*, t^*)$ when $t \neq t^*$.

Note that in the semi-parametric model of (2) and (3), only $\boldsymbol{\zeta}(\mathbf{s}, t)$, $\mathbf{x}(\mathbf{s})$ and $y(\mathbf{s}, t)$ are observed, but other quantities are kept unknown. The aim of this study is to predict the process $z(\mathbf{s}, t)$ by reconstructing those unknown terms $\boldsymbol{\alpha}$, \mathbf{W} , $\mathbf{f}(\mathbf{x}(\mathbf{s}))$ and $u(\mathbf{s}, t)$ based on $\mathbf{y}(\cdot, t)$, $t = 1, \dots, T$, as parsimonious as possible. To estimate those terms in (3), we begin with approximating $\boldsymbol{\alpha}$ using ordinary least squares (OLS), find \mathbf{W} and $\mathbf{f}(\mathbf{x}(\mathbf{s}))$ via

Pairwise Directions Estimation (PDE) proposed by Lue (2019), and then estimate $u(\mathbf{s}, t)$ by applying resolution adaptive fixed rank kriging, abbreviated as autoFRK, proposed by Tzeng and Huang (2018). We briefly introduce the two key building blocks, PDE and autoFRK, and then propose our estimation method in Section 2.3.

2.1 Pairwise Directions Estimation

We may treat the spatio-temporal data as a collection of time series $\{y(\mathbf{s}_i, 1), \dots, y(\mathbf{s}_i, T)\}$ at different locations. Suppose that $y(\mathbf{s}_i, t)$ for $i = 1, \dots, n; t = 1, \dots, T$, with a $P \times 1$ spatial-only covariate vector $\mathbf{x}(\mathbf{s}_i)$ and a $Q \times 1$ covariate vector $\boldsymbol{\zeta}(\mathbf{s}, t)$ are available. By assuming those time series being independent random replicates from an identical process, we apply PDE to the curve data model introduced by Li *et al.* (2003)

$$\check{y}(\mathbf{s}, t) = \sum_{j=1}^{\kappa} w_j(t) f_j(\boldsymbol{\theta}'_j \mathbf{x}(\mathbf{s})) + \gamma(\mathbf{s}, t), \quad (4)$$

for $t = t_1, \dots, t_T$, through regarding

$$\check{y}(\mathbf{s}, t) \equiv y(\mathbf{s}, t) - \sum_{i=1}^Q \hat{\alpha}_i \zeta_i(\mathbf{s}, t)$$

as the observed data with $\hat{\alpha}_i$ found by OLS. The “noise” $\gamma(\mathbf{s}, t)$ here is tentatively assumed to be independent, which plays a similar role as $u(\mathbf{s}, t) + \varepsilon(\mathbf{s}, t)$ in (2) and (3). The original setting for t_1, \dots, t_T is not necessarily equal-spaced, but for simplicity we assume them to be equal-spaced, and let $t_1 = 1, \dots, t_T = T$. We allow both \mathbf{w}_j and f_j to be determined by the data with the number κ as small as possible. The first term in (4) is used to approximate the second term in (3).

Let $\check{\mathbf{y}}(\cdot, t) = (\check{y}(\mathbf{s}_1, t), \dots, \check{y}(\mathbf{s}_n, t))'$, $\check{\mathbf{y}}(\mathbf{s}, \cdot) = (\check{y}(\mathbf{s}, 1), \dots, \check{y}(\mathbf{s}, T))'$, and $\check{\mathbf{Y}} = (\check{\mathbf{y}}(\cdot, 1), \dots, \check{\mathbf{y}}(\cdot, T))$. We apply two methods to obtain an initial estimate $\hat{\boldsymbol{\theta}}_j$ of $\boldsymbol{\theta}_j$, $j = 1, \dots, \kappa$, for efficiently implementing the PDE method. One choice is based on mrSIR method of Lue (2009). The initial $\boldsymbol{\theta}_j$ can be found by solving the generalized eigenvalue decomposition problem

$$\bar{\boldsymbol{\Psi}} \boldsymbol{\theta}_j = \rho_j \boldsymbol{\Sigma}_{\mathbf{x}} \boldsymbol{\theta}_j, \quad (5)$$

where $\bar{\boldsymbol{\Psi}} = \sum_{t=1}^T (\bar{\lambda}_t / \bar{\lambda}) \boldsymbol{\Psi}_t$, $\boldsymbol{\Psi}_t = \text{var}\{E(\mathbf{x}(\mathbf{s})) \check{\mathbf{y}}(\cdot, t)\}$, $\bar{\lambda}_t$ is the proportion of nonzero eigenvalues for the eigenvalue decomposition of $\boldsymbol{\Psi}_t$ with respect to $\boldsymbol{\Sigma}_{\mathbf{x}} = \text{var}(\mathbf{x}(\mathbf{s}))$ and $\bar{\lambda} = \sum_t \bar{\lambda}_t$.

Another choice is derived from pe-mrPHD method of Lue (2010) which is delineated as follows: It begins by forming the T principal components $\tilde{\mathbf{y}}_t$ from the $n \times T$ data matrix $\check{\mathbf{Y}}$ associated with eigenvalues λ_t , $t = 1, \dots, T$. Construct the covariance matrix $\boldsymbol{\Sigma}_{\tilde{\mathbf{y}}_t \mathbf{x}\mathbf{x}} = E\{\tilde{\mathbf{y}}_t(\mathbf{x}(\mathbf{s}) - E\mathbf{x}(\mathbf{s}))(\mathbf{x}(\mathbf{s}) - E\mathbf{x}(\mathbf{s}))'\}$ and let its eigenvalue decomposition be $\boldsymbol{\Phi}_t \text{diag}(\lambda_{1t}, \dots, \lambda_{Pt}) \boldsymbol{\Phi}'_t$, where $\boldsymbol{\Phi}_t = (\boldsymbol{\phi}_{1t}, \dots, \boldsymbol{\phi}_{Pt})$ and $\boldsymbol{\phi}_{it}$ is the eigenvector corresponding to eigenvalue λ_{it} for $i = 1, \dots, P$. Define a positive eigenvalue version for $\boldsymbol{\Sigma}_{\tilde{\mathbf{y}}_t \mathbf{x}\mathbf{x}}$ as $\check{\mathbf{H}}_t = \boldsymbol{\Phi}_t \text{diag}(|\lambda_{1t}|, \dots, |\lambda_{Pt}|) \boldsymbol{\Phi}'_t$, and let their weighted average be $\check{\mathbf{H}} = \sum_{t=1}^T (\lambda_t / \bar{\lambda}) \check{\mathbf{H}}_t$, where $\bar{\lambda} = \sum_{t=1}^T \lambda_t$. Then pe-mrPHD conducts the generalized eigenvalue decomposition of $\check{\mathbf{H}}$ with respect to $\boldsymbol{\Sigma}_{\mathbf{x}}$,

$$\check{\mathbf{H}} \boldsymbol{\theta}_j = \rho_j \boldsymbol{\Sigma}_{\mathbf{x}} \boldsymbol{\theta}_j, \quad (6)$$

to obtain $\hat{\boldsymbol{\theta}}_j$. Note that in (5) and (6), operations of $E(\cdot)$ and $\text{var}(\cdot)$ are done through the sample version in practice.

After initialization of $\boldsymbol{\theta}_j$, we utilize an adaptive estimation of MAVE (Xia *et al.*, 2002) for a single-index case to obtain initial estimate of \boldsymbol{w}_j by solving the minimization problem:

$$\min_{\tilde{d}_{j1}, \tilde{d}_{j2}, \boldsymbol{w}_j} \sum_{\ell=1}^n \sum_{i=1}^n \left(\boldsymbol{\theta}'_j \boldsymbol{x}(\boldsymbol{s}_i) - \{ \tilde{d}_{j1\ell} + \tilde{d}_{j2\ell} \boldsymbol{w}'_j (\check{\boldsymbol{y}}(\boldsymbol{s}_i, \cdot) - \check{\boldsymbol{y}}(\boldsymbol{s}_\ell, \cdot)) \} \right)^2 \delta_{i\ell}, \quad (7)$$

where $\delta_{i\ell} = K_{h_Y} \{ \boldsymbol{w}'_j (\check{\boldsymbol{y}}(\boldsymbol{s}_i, \cdot) - \check{\boldsymbol{y}}(\boldsymbol{s}_\ell, \cdot)) \} / \sum_{i=1}^n K_{h_Y} \{ \boldsymbol{w}'_j (\check{\boldsymbol{y}}(\boldsymbol{s}_i, \cdot) - \check{\boldsymbol{y}}(\boldsymbol{s}_\ell, \cdot)) \}$, K is a kernel function and h_Y is the bandwidth of $\check{\boldsymbol{y}}(\boldsymbol{s}, \cdot)$.

The iterative algorithm for estimating w_j , f_j , and $\boldsymbol{\theta}_j$ for $j = 1, \dots, \kappa$ in (4) via PDE proceeds in the following steps:

1. Choose initial estimates $\hat{\boldsymbol{\theta}}_{j(0)}$, $j = 1, \dots, \kappa$, from (5) and/or (6), and then get $\tilde{\boldsymbol{w}}_{j(0)}$ by (7). Compute the estimated bases $\hat{\boldsymbol{w}}_{j(0)} = \hat{\boldsymbol{\Sigma}}_{\check{\boldsymbol{y}}(\boldsymbol{s}, \cdot)} \tilde{\boldsymbol{w}}_{j(0)}$, where $\hat{\boldsymbol{\Sigma}}_{\check{\boldsymbol{y}}(\boldsymbol{s}, \cdot)}$ is the sample covariance of $\check{\boldsymbol{y}}(\boldsymbol{s}, \cdot)$ (see, Lemma of Lue (2019)).
2. At the τ -th iteration, fit a linear regression model to $\check{\boldsymbol{y}}(\boldsymbol{s}_i, \cdot)$ against $\{ \hat{\boldsymbol{w}}_{j(\tau-1)} \}_{j=1}^{\kappa}$, i.e. assuming

$$\check{\boldsymbol{y}}(\boldsymbol{s}_i, \cdot) = f_{1i} \hat{\boldsymbol{w}}_{1(\tau-1)} + \dots + f_{\kappa i} \hat{\boldsymbol{w}}_{\kappa(\tau-1)} + \boldsymbol{\varpi}(\boldsymbol{s}_i, \cdot), \quad (8)$$

for $i = 1, \dots, n$, to obtain the estimated coefficients $\hat{f}_{ji(\tau)}$, $j = 1, \dots, \kappa$, where the (τ) in the subscript denotes the iteration number.

3. Obtain the updated estimate $\tilde{\boldsymbol{w}}_{j(\tau)}$ from (7) by replacing $\boldsymbol{\theta}'_j \boldsymbol{x}(\boldsymbol{s}_i)$ with $\hat{f}_{ji(\tau)}$ and then compute the updated bases $\hat{\boldsymbol{w}}_{j(\tau)} = \hat{\boldsymbol{\Sigma}}_{\check{\boldsymbol{y}}(\boldsymbol{s}, \cdot)} \tilde{\boldsymbol{w}}_{j(\tau)}$, $j = 1, \dots, \kappa$.
4. Repeat steps 2 and 3 until $\| \hat{\boldsymbol{w}}_{j(\tau)} - \hat{\boldsymbol{w}}_{j(\tau-1)} \| < \Delta$, $j = 1, \dots, \kappa$, for some given tolerance value Δ (e.g., $\Delta = 0.001$).
5. Use the final estimate $\hat{\boldsymbol{w}}_j$ in step 4 to obtain the final estimates $\hat{\boldsymbol{\theta}}_j$ and \hat{f}_j , $j = 1, \dots, \kappa$, by solving the minimization problem:

$$\min_{d_{j1}, d_{j2}, \boldsymbol{\theta}_j} \sum_{\ell=1}^n \sum_{i=1}^n \left(\hat{\boldsymbol{w}}'_j \check{\boldsymbol{y}}(\boldsymbol{s}_i, \cdot) - \{ d_{j1\ell} + d_{j2\ell} \boldsymbol{\theta}'_j (\boldsymbol{x}(\boldsymbol{s}_i) - \boldsymbol{x}(\boldsymbol{s}_\ell)) \} \right)^2 \delta_{i\ell},$$

where $\delta_{i\ell} = K_{h_X} \{ \boldsymbol{\theta}'_j (\boldsymbol{x}(\boldsymbol{s}_i) - \boldsymbol{x}(\boldsymbol{s}_\ell)) \} / \sum_{i=1}^n K_{h_X} \{ \boldsymbol{\theta}'_j (\boldsymbol{x}(\boldsymbol{s}_i) - \boldsymbol{x}(\boldsymbol{s}_\ell)) \}$ and h_X is the bandwidth of $\boldsymbol{x}(\boldsymbol{s})$.

2.2 Resolution Adaptive Fixed Rank Kriging

The model of resolution adaptive fixed rank kriging represents $u(\boldsymbol{s}, t)$ as $u(\boldsymbol{s}, t) = \boldsymbol{m}(\boldsymbol{s})' \boldsymbol{q}(t)$, where $\boldsymbol{q}(t) \sim N(\mathbf{0}, \boldsymbol{\Omega})$ is independent over time and $\boldsymbol{m}(\boldsymbol{s}) = (m_1(\boldsymbol{s}), \dots, m_r(\boldsymbol{s}))'$ is the vector of r known basis functions defined in (9) below. Denote $\boldsymbol{\ell} = (1, \boldsymbol{s}')' = (1, s_1, \dots, s_d)'$. Then $m_k(\boldsymbol{s})$ is given by

$$m_k(\boldsymbol{s}) = \begin{cases} 1; & k = 1, \\ s_{k-1}; & k = 2, \dots, d+1, \\ s_{k-d-1}^{-1} \{ \boldsymbol{\beta}(\boldsymbol{s}) - \boldsymbol{B} \boldsymbol{L} (\boldsymbol{L}' \boldsymbol{L})^{-1} \boldsymbol{\ell} \}' \boldsymbol{p}_{k-d-1}; & k = d+2, \dots, n, \end{cases} \quad (9)$$

where $\mathbf{L} = (\boldsymbol{\ell}'_1, \dots, \boldsymbol{\ell}'_n)'$, $\boldsymbol{\beta}(\mathbf{s}) = (\beta_1(\mathbf{s}), \dots, \beta_n(\mathbf{s}))'$ with

$$\beta_i(\mathbf{s}) = \begin{cases} \frac{1}{12} \|\mathbf{s} - \mathbf{s}_i\|^3; & \text{if } d = 1, \\ \frac{1}{8\pi} \|\mathbf{s} - \mathbf{s}_i\|^2 \log(\|\mathbf{s} - \mathbf{s}_i\|); & \text{if } d = 2, \\ \frac{-1}{8} \|\mathbf{s} - \mathbf{s}_i\|; & \text{if } d = 3, \end{cases}$$

$\mathbf{B} = (\boldsymbol{\beta}(\mathbf{s}_1), \dots, \boldsymbol{\beta}(\mathbf{s}_n))$, \mathbf{p}_k is the k -th column of \mathbf{P} , and $\mathbf{P} \text{diag}(\varsigma_1, \dots, \varsigma_n) \mathbf{P}'$ is the eigen-decomposition of $(\mathbf{I} - \mathbf{L}(\mathbf{L}'\mathbf{L})^{-1}\mathbf{L}')\mathbf{B}(\mathbf{I} - \mathbf{L}(\mathbf{L}'\mathbf{L})^{-1}\mathbf{L}')$ with $\varsigma_1 \geq \dots \geq \varsigma_n$.

We can see that $m_k(\mathbf{s})$ is completely determined by $\{\mathbf{s}_1, \dots, \mathbf{s}_n\}$. Tzeng and Huang (2018) showed that $m_k(\mathbf{s})$ can be used to well approximate many nonstationary spatial processes. Our proposal assumes $E(y(\mathbf{s}, t)) = \boldsymbol{\alpha}'\boldsymbol{\zeta}(\mathbf{s}, t) + \mathbf{w}(t)\mathbf{f}(\mathbf{x}(\mathbf{s}))$. The parameters $\boldsymbol{\Omega}$ and $\sigma_\varepsilon^2(t) \equiv \sigma^2$ for a given set of $m_1(\mathbf{s}), \dots, m_r(\mathbf{s})$ can be estimated via a closed-form maximum likelihood estimation based on the ‘‘residuals’’

$$e(\mathbf{s}, t) \equiv y(\mathbf{s}, t) - \hat{\boldsymbol{\alpha}}'\boldsymbol{\zeta}(\mathbf{s}, t) - \hat{\mathbf{w}}(t)\hat{\mathbf{f}}(\mathbf{x}(\mathbf{s})),$$

according to the solution given in Tzeng and Huang (2018), where $\hat{\mathbf{w}}(t)$ and $\hat{\mathbf{f}}(\mathbf{x}(\mathbf{s})) = (\hat{f}_1(\hat{\boldsymbol{\theta}}'_1\mathbf{x}(\mathbf{s})), \dots, \hat{f}_r(\hat{\boldsymbol{\theta}}'_r\mathbf{x}(\mathbf{s})))'$ are obtained by PDE.

$$\hat{\sigma}^2 = \max \left\{ \frac{\text{tr}(\mathbf{S}) - \sum_{k=0}^N \xi_k}{n - N}, 0 \right\}, \quad (10)$$

$$\hat{\boldsymbol{\Omega}} = (\mathbf{M}'\mathbf{M})^{-1/2} \mathbf{V} \text{diag}(\hat{\xi}_1, \dots, \hat{\xi}_r) \mathbf{V}' (\mathbf{M}'\mathbf{M})^{-1/2}, \quad (11)$$

where $(S)_{ij} = \frac{1}{T} \sum_{t=1}^T e(\mathbf{s}_i, t)e(\mathbf{s}_j, t)$, $\mathbf{M} = (\mathbf{m}(\mathbf{s}_1), \dots, \mathbf{m}(\mathbf{s}_n))'$,

$$\begin{aligned} \mathbf{V} \text{diag}(\xi_1, \dots, \xi_r) \mathbf{V}' &= (\mathbf{M}'\mathbf{M})^{-1/2} \mathbf{M}' \mathbf{S} \mathbf{M} (\mathbf{M}'\mathbf{M})^{-1/2}, \\ N &= \max \left(\{0\} \cup \left\{ J : \xi_J > \frac{\text{tr}(\mathbf{S}) - \sum_{k=0}^J \xi_k}{n - J}; J = 1, \dots, r \right\} \right), \end{aligned}$$

$\xi_0 = 0$, and $\hat{\xi}_k = \max(\xi_k - \hat{\sigma}^2, 0)$ for $k = 1, \dots, r$. Moreover, the optimal number of r is chosen via Akaike’s information criterion. Once r is chosen, the final predictor for $u(\mathbf{s}, t)$ is given by

$$\hat{u}(\mathbf{s}, t) = \mathbf{m}(\mathbf{s})\hat{\boldsymbol{\Omega}}\mathbf{M}(\mathbf{M}\hat{\boldsymbol{\Omega}}\mathbf{M}' + \hat{\sigma}^2\mathbf{I}_n)^{-1}\mathbf{e}(\cdot, t),$$

with $\mathbf{e}(\cdot, t) = (e(\mathbf{s}_1, t), \dots, e(\mathbf{s}_n, t))'$.

2.3 PDE+

We propose a new enhanced method of PDE, called PDE+, through incorporating the PDE with autoFRK for modeling spatio-temporal data. In what follows, $\mathbf{e}(\mathbf{s}, \cdot)$, $\hat{\mathbf{e}}(\mathbf{s}, \cdot)$, $\mathbf{u}(\mathbf{s}, \cdot)$, and $\hat{\mathbf{u}}(\mathbf{s}, \cdot)$ are defined in a similar way as $\check{\mathbf{y}}(\mathbf{s}, \cdot)$ with respect to $\{\check{y}(\mathbf{s}, t); t = 1, \dots, T\}$. The algorithm for PDE+ proceeds in the following steps:

- I. Use OLS on the learning data $\{\boldsymbol{\zeta}(\mathbf{s}, \cdot), \mathbf{y}(\mathbf{s}, \cdot)\}$ to get the estimate $\hat{\boldsymbol{\alpha}}$, and then obtain $\check{\mathbf{y}}(\mathbf{s}, \cdot)$.
- II. Apply PDE to the data $\{\mathbf{x}(\mathbf{s}), \check{\mathbf{y}}(\mathbf{s}, \cdot)\}$ for obtaining $\hat{\mathbf{f}}(\mathbf{x}(\mathbf{s}))$ and $\{\hat{\mathbf{w}}_j\}_{j=1}^r$, and then get the residuals $\mathbf{e}(\mathbf{s}_i, \cdot)$ from a linear fit of $\check{\mathbf{y}}(\mathbf{s}, \cdot)$ against $\{\hat{\mathbf{w}}_j\}_{j=1}^r$ for $i = 1, \dots, n$. Use autoFRK in Section 2.2 on $\mathbf{e}(\mathbf{s}, \cdot)$ to approximate $\mathbf{u}(\mathbf{s}, \cdot)$.

III. Let $\hat{e}(\mathbf{s}, \cdot)$ be the difference between $\check{\mathbf{y}}(\mathbf{s}, \cdot)$ and $\hat{\mathbf{u}}(\mathbf{s}, \cdot)$ from step II, and then repeat step II once by treating the learning data as $\{\mathbf{x}(\mathbf{s}), \hat{e}(\mathbf{s}, \cdot)\}$.

We call both steps I and II in this algorithm as loop.0, and all steps as loop.1. The final predictive model of PDE+ is defined as the one with the minimum learning prediction error among loop.0, loop.1 and PDE in Section 2.1. The reason for taking once iteration on PDE+ is for computational efficiency.

3 Numeric Results

3.1 Simulation Setups

Suppose that we observe data $y(\mathbf{s}, t)$ at location \mathbf{s} and time t . Let the spatial-only covariate vector be $\mathbf{x}(\mathbf{s}) = (s_1, s_2, s_1^2, s_2^2)'$, where $\mathbf{s} = (s_1, s_2)'$, generated from given spatial locations and $f_j(\cdot)$ be the coefficient function for unknown spatial structure shared across t . Under (2) and (3), we think of $\mathbf{w}(t)\mathbf{f}(\mathbf{x}(\mathbf{s}))$ as deterministic, or fixed effects. In addition to generating data from such a model, we are also curious about the robustness of PDE+ under a stochastic setting of $\mathbf{w}(t)\mathbf{f}(\mathbf{x}(\mathbf{s}))$. Therefore, we consider three simulation scenarios for such observations as follows:

(s1). Assume $u(\mathbf{s}, t) = 0$, while $\boldsymbol{\alpha}'\boldsymbol{\zeta}(\mathbf{s}, t)$ is a constant and $w_j(t)$ are deterministic but unknown smooth functions.

(s2). Assume $u(\mathbf{s}, t) = 0$ and $w_j(t) = \rho w_j(t-1) + \eta_j(t)$ for some ρ with $|\rho| < 1$, where $\eta_j(t)$ is a white noise with mean zero and variance $\sigma_\eta^2(t)$ independent over t and j .

(s3). Assume $\mathbf{w}(t) = \mathbf{w}(t-1)\mathbf{G} + \boldsymbol{\eta}(t)'$ in an autoregressive manner with a common but unknown \mathbf{G} and temporally independent of $\boldsymbol{\eta}(t) \sim N(\mathbf{0}, \boldsymbol{\Sigma}_\eta)$, and $u(\mathbf{s}, t)$'s are spatial random effects independent over time, i.e. $\text{cov}(u(\mathbf{s}, t), u(\mathbf{s}^*, t^*)) = \sigma_u^2 \exp(-c\|\mathbf{s} - \mathbf{s}^*\|)$ if $t = t^*$; 0, otherwise. Also, we need the initialization of $\mathbf{w}(0)'$ from $N(\mathbf{0}, \mathbf{C}_0)$.

We apply our proposed method to dimension reduction for studying predictive modeling on spatio-temporal data through simulated examples. To evaluate the performance of model prediction among various methods, we compute two versions of prediction error criteria, namely root integrated mean squared error (RIMSE) and rooted prediction mean squared error (RPMSE), defined by

$$\begin{aligned} \text{RIMSE} &= \frac{1}{n_t} \sum_{i=1}^{n_t} \|\mathbf{y}(\mathbf{s}_i, \cdot) - \hat{\mathbf{z}}(\mathbf{s}_i, \cdot)\|, \\ \text{RPMSE} &= \left(\frac{1}{n_t T} \sum_{t=1}^T \sum_{i=1}^{n_t} (y(\mathbf{s}_i, t) - \hat{z}(\mathbf{s}_i, t))^2 \right)^{1/2}, \end{aligned} \quad (12)$$

where n_t is the size of locations in the testing data, $\hat{z}(\mathbf{s}_i, t)$ denotes the estimate of $z(\mathbf{s}_i, t)$, and $\hat{\mathbf{z}}(\mathbf{s}_i, \cdot) = (\hat{z}(\mathbf{s}_i, 1), \dots, \hat{z}(\mathbf{s}_i, T))'$. The cross-validation estimates of RIMSE and RPMSE for each example are collected over 100 replications. The performance is then compared with four methods, referred to as naive, spTimer, kriging and mgcv, which are briefly reviewed below.

The naive method is the simplest predictor $\hat{z}(\mathbf{s}, t) = \frac{1}{n_t} \sum_{i=1}^{n_t} y(\mathbf{s}_i, t)$, i.e., the sample mean of all locations at time t . The spTimer method uses hierarchical Bayesian modeling for space-time data. Its model is given by

$$\begin{aligned} y(\mathbf{s}, t) &= \alpha + R(\mathbf{s}, t) + \varepsilon(\mathbf{s}, t) \\ R(\mathbf{s}, t) &= \rho R(\mathbf{s}, t-1) + u(\mathbf{s}, t), \end{aligned}$$

where $u(\mathbf{s}, t)$'s are mean-zero spatial random effects independent over time with an isotropic stationary Matérn covariance function. This method has been implemented in an R package named `spTimer`. The kriging method is based on a standard spatio-temporal interpolation procedure. It assumes that the data comes from $y(\mathbf{s}, t) = \mu(t) + u(\mathbf{s}, t) + \varepsilon(\mathbf{s}, t)$, where $u(\mathbf{s}, t)$ is a mean-zero second order stationary stochastic process with a product-sum spatial-temporal covariance in the form

$$C_{st}(h_s, h_t) = k_1 C_s(h_s) C_t(h_t) + k_2 C_s(h_s) + k_3 C_t(h_t)$$

for any pair of space-time points (\mathbf{s}, t) and $(\mathbf{s} + h_s, t + h_t)$, with $C_s(h_s)$ and $C_t(h_t)$ valid covariance functions. There are various covariance models, and we use the product-sum model in view of its flexibility and widespread applications in many areas. The `mgcv` method exploits additive models with tensor products. It assumes

$$E[y(\mathbf{s}, t)] = g_1(s_1) + g_2(s_2) + g_3(t) + g_4(s_1, s_2) + g_5(s_1, t) + g_6(s_2, t) + g_7(s_1, s_2, t), \quad (13)$$

where g_k 's are constructed by superimposing several known basis functions and its noises are assumed to follow $N(0, \Sigma_\eta)$ independently over space and time. With these higher-order interactions, the model tends to overfit, and hence some penalized approach is necessary. The famous R package `mgcv` provides convenient ways for determining an appropriate penalty.

According to their algorithms, the default values are used to set the turning parameters. We emphasize the accuracy of estimating the prediction error in (12) and the findings of the interesting pattern structures. From simulations and practical applications in the next two sections, PDE successfully achieves the accuracy of the EDR direction estimation.

3.2 Comparison of Simulation Results

In each simulation run, we set $T = 20$ and generate $\mathbf{y}(\mathbf{s}_i, \cdot)$ at $n = 150$ locations which consist of a learning data with size 120 and a testing data with size 30. We set the number of slices for `mrSIR` to be 10.

Example 1. Under (s1). We consider a spatial process, $\{z(\mathbf{s}, t) : \mathbf{s} \in [-1, 1]^2\}$, generated from (3) with $\alpha = 0$,

$$\begin{aligned} f_1(\mathbf{s}) &= \cos(0.5\pi\|\mathbf{s} - (-0.5, -0.5)'\|^2), \\ f_2(\mathbf{s}) &= \sin(0.5\pi\|\mathbf{s} - (0.5, 0.5)'\|^2), \end{aligned} \quad (14)$$

$$w_1(t) = (0.2t - 2)^2, \quad w_2(t) = \sin(0.1\pi t), \quad (15)$$

for $t = 1, \dots, T$. According to (2), the data $\{\mathbf{y}(\mathbf{s}_i, \cdot); i = 1, \dots, 150\}$ with $\sigma_\varepsilon^2(t) = [t/(c \times T)]^2$ (i.e. $\sigma_\varepsilon^2(t) \leq 1/c^2, \forall t$) are generated. The location set $\{\mathbf{s}_1, \dots, \mathbf{s}_n\}$ is drawn from $\mathcal{D} = [-1, 1]^2$ using simple random sampling. With letting $\boldsymbol{\theta}_1 = (0.5, 0.5, 0.5, 0.5)'$ and $\boldsymbol{\theta}_2 = (-0.5, -0.5, 0.5, 0.5)'$, the coefficient functions f_j 's can be reformulated as $f_1(\mathbf{s}) = \cos(0.5\pi(2\boldsymbol{\theta}_1'\mathbf{x}(\mathbf{s}) + 0.5))$ and $f_2(\mathbf{s}) = \sin(0.5\pi(2\boldsymbol{\theta}_1'\mathbf{x}(\mathbf{s}) + 0.5))$. Both unknown vectors, $\boldsymbol{\theta}_1$ and $\boldsymbol{\theta}_2$, are sufficient dimension reduction directions needed to be estimated. This data contain trigonometric and quadratic features.

To illustrate the application of PDE via data visualization, a single run is taken for high-noise case, $c = 2$. The data are generated according to models (14) and (15). We separately conduct the eigenvalue decomposition in (5) and (6) for the learning data to obtain initial estimates $\hat{\boldsymbol{\theta}}_j$'s. It turns out that the modified eigenvalues (0.55, 0.28,

0.03, 0) found by mrSIR suggest one $\mathbf{x}(\mathbf{s})$ variate. One significant direction is also found by pe-mrPHD with the eigenvalues (1.35, 0.84, 0.28, 0.13). By choosing $h_Y = 2, h_{\mathbf{x}} = 0.5$ and taking the two initial estimates $\hat{\boldsymbol{\theta}}_j, j = 1, 2$, we proceed with the PDE algorithm to dimension reduction for $\mathbf{x}(\mathbf{s}_i)$ and $y(\mathbf{s}_i, t), i = 1, \dots, n; t = 1, \dots, T$. After attaining the iterative convergence, two leading directions, $(0.497, 0.505, 0.495, 0.502)'$ and $(-0.491, -0.506, 0.495, 0.507)'$, for $\mathbf{x}(\mathbf{s})$ variates are found which are consistent with the theoretical vectors $\boldsymbol{\theta}_j$'s. Our work of the PDE is satisfactory with $R^2(\hat{\boldsymbol{\theta}}_1) = 0.993$ and $R^2(\hat{\boldsymbol{\theta}}_2) = 0.987$, where $R^2(\hat{\boldsymbol{\theta}}_j)$ denotes the squared correlation between $\boldsymbol{\theta}_j' \mathbf{x}(\mathbf{s})$ and $\hat{\boldsymbol{\theta}}_j' \mathbf{x}(\mathbf{s})$. The scatterplot of the first estimated coefficient function, shown in Figure 1(A), reveals a noticeable quadratic pattern. Figure 1(B) shows a clear sine pattern for the second estimated coefficient function. Figures 1(C) and 1(D) display basis functions which are very close to the true patterns.

Under (3) with letting $u(\mathbf{s}, t) = 0$, similar to (8), we use $\sum_{j=1}^{\kappa} b_j(\mathbf{s}_i) \hat{f}_{ji} \hat{\boldsymbol{w}}_j$ to approximate $\check{\mathbf{y}}(\mathbf{s}_i, \cdot)$ based on a linear fit for scaling $\hat{\mathbf{f}}(\mathbf{x}(\mathbf{s}))$, where b_j is a $n \times 1$ vector. Then the estimates $(\hat{b}_j(\mathbf{s}_1) \hat{f}_{j1}, \dots, \hat{b}_j(\mathbf{s}_n) \hat{f}_{jn})', j = 1, \dots, \kappa$, are the scaled coefficients. As a matter of fact, the scaling does not have an influence on the structure of coefficients; it would improve the prediction accuracy instead. In calculating $\hat{\mathbf{z}}(\mathbf{s}_0, \cdot)$ for \mathbf{s}_0 in the testing data, $\hat{b}_j(\mathbf{s}_0) \hat{f}_{j0}$ can be obtained by using the average of k-nearest neighbors around \mathbf{s}_0 in the learning data. In general, based on the testing data and our final estimates, i.e. $\hat{b}_j(\mathbf{s}) \hat{f}_j$ and $\hat{\boldsymbol{w}}_j$ for $j = 1, \dots, \kappa$ ($\hat{u}(\mathbf{s}, t)$ will be used for prediction in Example 3), the RIMSE = 1.294 and PMSE = 0.296 are found by PDE in the single run.

In reference to the sampling performance, the results based on 100 simulated replicates according to (14) and (15) are summarized in Table 1. It reports the mean and standard deviation for RIMSE and PMSE found by all methods. PDE does outperform with the smallest averaged prediction error values for the model in scenario 1, and even better for low-noise case (i.e. $c = 10$) because of more clear signal for functional patterns. The mean of RIMSE obtained by PDE is only 0.610, which is about 54.2% ($= 0.941/0.610 - 1$) improvement over kriging. Not surprisingly, PDE uses locally linear information via smoothing techniques to capture the function forms of \boldsymbol{w}_j and $f_j, j = 1, \dots, \kappa$. Regarding the predictive modeling, PDE introduces dimension reduction steps to catch the $\mathbf{x}(\mathbf{s})$ variates for improving model fitting.

Example 2. Under (s2), a model setting considered is the same as the one in Example 1, except that $w_j(t)$ is stochastic and set to be

$$w_j(t) = 0.8 w_j(t-1) + \eta_j(t), \quad (16)$$

with $\sigma_{\eta}^2(t) = 0.5$. Based on (2), the data $\{\mathbf{y}(\mathbf{s}_i, \cdot); i = 1, \dots, 150\}$ are generated with $\sigma_{\varepsilon}^2(t) = (t/10)^2$. Both $\boldsymbol{\theta}_1 = (0.5, 0.5, 0.5, 0.5)'$ and $\boldsymbol{\theta}_2 = (-0.5, -0.5, 0.5, 0.5)'$ are two important directions for dimension reduction similarly.

A single run is taken for the generated data from models (14) and (16) by proceeding the same procedures as in Example 1. It shows that mrSIR suggests one $\mathbf{x}(\mathbf{s})$ variate indicated by the modified eigenvalues (0.42, 0.18, 0, 0) and another significant direction is found by pe-mrPHD with the eigenvalues (2.93, 2.01, 0.61, 0.03). After attaining the iterative convergence, two leading directions for $\mathbf{x}(\mathbf{s})$ variates, $(0.509, 0.500, 0.505, 0.485)'$ and $(-0.497, -0.492, 0.499, 0.510)'$, are found by taking $h_Y = 0.5, h_{\mathbf{x}} = 0.5$. The scatterplots of the first two estimated coefficient functions, shown in Figures 2(A) and 2(B), reveal clear quadratic and sine patterns, even though Figures 2(C) and 2(D) exhibit vague pictures for basis functions.

The results based on 100 simulation runs according to models (14) and (16) are summarized in Table 2. For predictive accuracy, the dominating values of simulation

results show that PDE+ has a competitive performance compared with kriging. In contrast, the naive, spTimer and mgcv produce considerable mean squared error in estimation, however.

Example 3. Under (s3). Consider two spatio-temporal covariates,

$$\begin{aligned}\zeta_1(\mathbf{s}, t) &= s_1 \cdot s_2 + \pi \log\left(\frac{t+1}{t}\right), \\ \zeta_2(\mathbf{s}, t) &= s_1^2 + s_2^2 - \sqrt{t},\end{aligned}$$

for $\mathbf{s} = (s_1, s_2)' \in \mathfrak{R}^2$. A spatial process $\{z(\mathbf{s}, t) : \mathbf{s} \in [-1, 1]^2\}$ is generated from (3) but with stochastic $\mathbf{w}(t)$:

$$\begin{aligned}\boldsymbol{\alpha}'\boldsymbol{\zeta}(\mathbf{s}, t) &= 3 + \zeta_1(\mathbf{s}, t) - 2\zeta_2(\mathbf{s}, t), \\ \mathbf{w}(t) &= \mathbf{w}(t-1)\mathbf{G} + \boldsymbol{\eta}(t)', \\ \begin{pmatrix} u(\mathbf{s}, t) \\ u(\mathbf{s}^*, t^*) \end{pmatrix} &\sim N\left(\begin{bmatrix} 0 \\ 0 \end{bmatrix}, \begin{bmatrix} 0.25 & \sigma_{\mathbf{s}, \mathbf{s}^*} \\ \sigma_{\mathbf{s}, \mathbf{s}^*} & 0.25 \end{bmatrix}\right),\end{aligned}\tag{17}$$

where $\mathbf{G} = \begin{bmatrix} 0.7 & -0.11 \\ 0.1 & 0.77 \end{bmatrix}$, $\boldsymbol{\Sigma}_\eta = \text{diag}(0.15, 0.15)$, $\sigma_{\mathbf{s}, \mathbf{s}^*} = \text{cov}(u(\mathbf{s}, t), u(\mathbf{s}^*, t^*)) = 0.25 \exp(-0.5\|\mathbf{s} - \mathbf{s}^*\|)$ if $t = t^*$; 0, otherwise, and $\mathbf{C}_0 = \text{diag}(5, 5)$. The noise variance $\sigma_\epsilon^2(t)$ is set to be 0.15.

The data for a single run are generated from models (14) and (17). The mrSIR suggests one $\mathbf{x}(\mathbf{s})$ variate shown by the modified eigenvalues (0.40, 0.16, 0.01, 0) and another significant direction is found by pe-mrPHD with the eigenvalues (1.41, 1.17, 0.68, 0.12). First of all, the estimated parameter vector for $\mu(\mathbf{s}, t)$ found by OLS are (3.224, 0.656, -1.926) which deviates from the theoretical vector (3, 1, -2)'. Two leading directions for $\mathbf{x}(\mathbf{s})$ variates, (0.539, 0.539, 0.494, 0.418)' and (-0.483, -0.430, 0.596, 0.475)', are found by taking $h_Y = 1$, $h_x = 0.5$, after attaining the iterative convergence. The scatterplots of the first two estimated coefficient functions, shown in Figures 3(A) and 3(B), reveal clear quadratic and sine patterns, even though Figures 3(C) and 3(D) exhibit vague pictures for basis functions. Note that the setup for $\mathbf{w}(t)$ here is more complicated than that in Example 2, since the behavior of two basis functions $w_1(t)$ and $w_2(t)$ is interlaced due to a non-zero correlation. Because PDE+ does not make use of the correlation structure of $\mathbf{w}(t)$, it may lose some efficiency for its estimate of $\mathbf{w}(t)$. Also, the random effect $u(\mathbf{s}, t)$ has a perturbative impact on the estimation of $\mathbf{f}(\mathbf{x}(\mathbf{s}))$ for PDE+.

The results based on 100 simulation runs according to models (14) and (17) are summarized in Table 3. For predictive accuracy, the dominating values of simulation results show that PDE+ has a competitive performance compared to other methods except for kriging. However, kriging is notoriously computation intensive, while all other methods can be viewed as computationally efficient alternatives to kriging. PDE slightly works better than PDE+ on the average perspective. In contrast, the naive, spTimer and mgcv produce considerable mean squared error in estimation, however.

Based on the results of Examples 2 and 3, the improvement of model prediction for PDE+ is comprehensible. When the pattern of $\mathbf{w}(t)$ is not smooth enough, autoFRK can enhance the accuracy of its estimation for $\mathbf{w}(t)\mathbf{f}(\mathbf{x}(\mathbf{s}))$. In case PDE works well enough, the model complexity would cause PDE+ to slightly produce larger prediction error compared to PDE. As this example illustrates, such cost PDE+ has to take is acceptable.

4 Applications to Real Data

To illustrate the application of our approach to predictive modeling for empirical studies, we analyze two real datasets. In the following datasets, the longitudes and latitudes are available for given spatial locations. Let the spatial-only covariate vector be $\mathbf{x}(\mathbf{s}) = (s_1, s_2, s_1^2, s_2^2)'$, where s_1 is the longitude and s_2 is the latitude. Also $\{\zeta_i(\mathbf{s}, t) = \mathbb{I}(t = i); i = 1, \dots, T\}$ is simply used.

4.1 Canadian Weather Data

We applied the proposed method to a dataset of average temperatures over the years 1960 to 1994 for each day of the year at 35 weather stations in Canada. The data are available in the `fd` package on Comprehensive R Archive Network (CRAN). The response data $y(\mathbf{s}, t)$ of interest are the average of temperatures measured on 35 location sites for 365 days. The map of observation locations is shown in Figure 4(B).

The annual temperature cycle at 35 stations shown in Figure 4(A) indicates a clear concave-down pattern. We first standardize $\mathbf{x}(\mathbf{s})$ for being centered and removing scale for further analysis. We conduct the eigenvalue decomposition in (6) for the learning data to obtain initial estimates $\hat{\boldsymbol{\theta}}_j$'s. Two significant directions are found by pe-mrPHD with the eigenvalues (3.23, 2.45, 1.80, 1.02). By choosing the bandwidths, $h_Y = 3$ and $h_{\mathbf{x}} = 1$, we proceed with the PDE algorithm to dimension reduction for $\mathbf{x}(\mathbf{s}_i)$ and $y(\mathbf{s}_i, t)$, $i = 1, \dots, 35$; $t = 1, \dots, 365$. After convergence, two leading directions are $(-0.109, -0.944, 0.221, -0.217)'$ and $(-0.297, -0.111, -0.904, -0.284)'$. It shows that there exists respective dominant effects, *latitude* and *squared longitude*, for the first two variates.

According to (3), the basis functions $w_j(t)$ and coefficients $f_j(\boldsymbol{\theta}_j \mathbf{x}(\mathbf{s}))$ affect the response $z(\mathbf{s}, t)$ through their inner product form. Figures 4(C) and 4(D) display the estimated basis functions which reveal similar concave-down patterns. From Figure 4(C), \hat{w}_1 is negative but has much higher values in summer shown in the middle of the horizontal axis (Day) and the lower values in winter at the left and right sides of the plot. Note that \hat{f}_1 in Figure 4(E) has positive values for a great portion of $\hat{\boldsymbol{\theta}}_1' \mathbf{x}(\mathbf{s})$, where large (small) values of $\hat{\boldsymbol{\theta}}_1' \mathbf{x}(\mathbf{s})$ represents southern (northern) locations due to the dominant negative standardized latitude values in $\hat{\boldsymbol{\theta}}_1$. Thus the dominant component $\hat{w}_1(t) \hat{f}_1(\hat{\boldsymbol{\theta}}_1 \mathbf{x}(\mathbf{s}))$ just goes consistently with the common sense that the larger latitude is, the lower temperature is in winter; the lower latitude is, the higher temperature is in summer. The left end of Figure 4(F) is around Newfoundland and Labrador while the right end corresponds to Yukon and British Columbia since the negative squared longitude is roughly dominant to the (standardized) horizontal axis. The shape of \hat{w}_2 roughly contrasts the temperature difference between summer and winter, due to the two seasons having the opposite signs of the function value. Therefore $\hat{w}_2(t) \hat{f}_2(\hat{\boldsymbol{\theta}}_2 \mathbf{x}(\mathbf{s}))$ shows a secondary component that the temperature difference in the middle of Canada is approximately half of that in the east or west coasts. Given locations with similar temperatures in summer shown in Figures 4(A), the secondary component implies that coastal areas tend to have lower temperature in winter, compared to the continental regions at the similar latitude.

In reference to the sampling performance, the results based on 100 randomly data partition are summarized in Table 4. In each of 100 analysis runs, we randomly partition $\{\mathbf{y}(\mathbf{s}_i, \cdot); i = 1, \dots, 35\}$ into a learning data with size 30 and a testing data with size 5. The large value of RIMSE or RPMSE found by `mgcv` indicates its heavy overfitting. Another analysis based on `mgcv` with stronger smoothness constraints, via basically dropping the g_7 term in (13), gives a better result; namely, a mean of 73.51 with a standard error 72.60 for RIMSE and a mean of 5.128 with a standard error 6.473 for RPMSE. It

should be aware of the constraint impact on the model complexity, even though mgcv provides automatic penalty determination. The PDE+ does outperform with the smallest averaged prediction error because of its finding of clear functional patterns. The mean of RIMSE obtained by PDE+ is only 44.24, which is about 115% ($= 95.32/44.24 - 1$) improvement over kriging. Not unexpectedly, PDE indeed captures the similarly concave-down patterns for function forms of $w_j(t)$ and $f_j(\boldsymbol{\theta}_j \mathbf{x}(\mathbf{s}))$, $j = 1, 2$, useful for improving model prediction.

4.2 Italy Cigarette Data

A dynamic spatial panel data about cigarette diffusion in Italy over the period 1877-1913 was considered (for access to the data, see Ciccarelli and Elhorst (2018)). The response data $y(\mathbf{s}, t)$ of concern are the levels of per capita consumptions measured on 69 provinces for 37 years. The map of observation locations is shown in Figure 5(B). We also first standardize $\mathbf{x}(\mathbf{s})$ for further analysis.

The levels of per capita consumptions at 69 provinces shown in Figure 5(A) indicates a clear increasing pattern. Two significant directions are found by pe-mrPHD with the eigenvalues (3.60, 3.18, 1.17, 0.40) for the eigenvalue decomposition in (6). After the convergence of PDE algorithm, two leading directions, $(-0.768, 0.046, -0.585, -0.260)'$ and $(0.375, 0.840, -0.333, -0.208)'$, for $\mathbf{x}(\mathbf{s})$ variates are found by choosing $h_Y = 1$ and $h_x = 0.5$. It reveals that there exist respectively dominant effects; namely, *longitude* and *squared longitude* for the first variate, and *latitude* for the second variate.

Figures 5(C) and 5(D) display the estimated basis functions which reveal similar increasing patterns, although some occasionally sharp changes appear. Note that \hat{w}_1 is negative shown in Figure 5(C). Since $\hat{\boldsymbol{\theta}}_1' \mathbf{x}(\mathbf{s})$ is basically proportional to negative longitude value, Figure 5(E) indicates that the closer to the west side is, the value of coefficient function gets smaller, and also shows that there are two major peaks in \hat{f}_1 . That implies the level of cigarette consumption for western (or mid-longitude) areas gets larger increase due to the inner-product effect in (3). The opposite signs on the left and the right parts of the horizontal axis in Figure 5(D) indicate that \hat{w}_2 roughly reveals the contrast of log per capita consumption between after and before 1895. Because real income increased rapidly from 1895 to 1913, it led to the famous period called belle époque. Figures 5(F) displays a plateau around the middle of the horizontal axis, $\hat{\boldsymbol{\theta}}_2' \mathbf{x}(\mathbf{s})$, which reflects roughly the latitude effect. Hence, $\hat{w}_2(t) \hat{f}_2(\hat{\boldsymbol{\theta}}_2' \mathbf{x}(\mathbf{s}))$ approximately indicates that mid-latitude areas have the largest increase during the belle époque.

The results based on 100 randomly data partition for sampling performance are summarized in Table 5. In each of 100 analysis runs, we randomly partition $\{\mathbf{y}(\mathbf{s}_i, \cdot); i = 1, \dots, 69\}$ into a learning data with size 60 and a testing data with size 9. PDE+ works well with the smallest averaged prediction error; however, kriging has surprisingly almost no advantage over the naive method for this data, and mgcv is also prone to overfitting. In the aspect of predictive accuracy, the mean of RIMSE obtained by PDE+ is only 3.461, which is about 8.23% ($= 3.746/3.461 - 1$) improvement over spTimer. Though PDE indeed captures the substantial patterns for function forms of $w_j(t)$ and $f_j(\boldsymbol{\theta}_j \mathbf{x}(\mathbf{s}))$, $j = 1, 2$, ignoring $u(\mathbf{s}, t)$ makes its prediction unsatisfactory. PDE+ properly incorproates the spatial random effects via $\hat{u}(\mathbf{s}, t)$, which is evidently useful for improving model prediction. More importantly, PDE+ can greatly help the explanation of the spatio-temporal trends, which is difficult for all other methods.

5 Discussion

Though variable selection was less paid attention to most of spatio-temporal data analysis in the past, variable selection for geostatistics is crucial in order to skip any perturbation from irrelevant variables. Classical variable selection theories are not applicable due to the violation of independent assumption between observations. Recently some research works for variable selection in dependent data are developed. For example, Joseph, Hung, and Sudjianto (2008) proposed a Bayesian method with cross validation to select useful variables for the mean function; Huang and Chen (2007) introduced a data-adaptive optimal approach for model selection through data perturbation. Both methods are computationally intensive, however.

A more challenging question is how to detect (or take into account) an important covariate which is linearly or nonlinearly associated with the spatio-temporal variable of interest. Some analysts may use a brute-force, but not recommended, strategy to generate plenty of transformed variables from covariates, and then select the appropriate ones using a classical variable selection procedure for model building. Our proposed method based on dimension reduction provides an alternative way to determine not only important variables but also the associated functional forms. Our results show that the proposed method can successfully incorporate important spatial-only covariate of $\mathbf{x}(\mathbf{s})$ through $\boldsymbol{\theta}$ efficiently, and its performance is quite robust even if $w_j(\mathbf{s})$ is stochastic. One future topic of research is how to extend such dimension reduction to spatio-temporal covariates, i.e., $\zeta(\mathbf{s}, t)$'s.

Missing data often occur in practical problems. Methods based on Monte Carlo expectation-maximization or multiple imputation could be a way out, but the cost of intensive computation raises another issue for large n and/or large T . Such problem requires more efforts in future research study.

ACKNOWLEDGEMENTS

Lue's and Tzeng's research works were supported in part by grants from the Ministry of Science and Technology of Taiwan MOST107-2118-M-029-001, and MOST 107-2118-M-110-004-MY3, respectively. We thank Professor Hsin-Cheng Huang for useful comments greatly improving the article.

REFERENCES

- Braud, I., and Obled, C. (1991), "On the use of Empirical Orthogonal Function (EOF) analysis in the simulation of random fields," *Stochastic Hydrology and Hydraulics*, 5, 125-134.
- Coudret, R., Girard, S., and Saracco, J. (2014), "A new sliced inverse regression method for multivariate response," *Computational Statistics & Data Analysis*, 77, 285-299.
- Cressie, N., and Johannesson, G. (2008), "Fixed rank kriging for very large spatial data sets," *Journal of the Royal Statistical Society: Series B (Statistical Methodology)*, 70, 209-226.
- Cressie, N., Shi, T., and Kang, E. L. (2010), "Fixed rank filtering for spatio-temporal data," *Journal of Computational and Graphical Statistics*, 19, 724-745.
- Cressie, N. and Wikle, C. K. (2011), *Statistics for Spatio-Temporal Data*, Hoboken, NJ: John Wiley & Sons.
- Demsar, U., Harris, P., Brunson, C., Fotheringham, A. S., and McLoone, S. (2013), "Principal component analysis on spatial data: an overview," *Annals of the Association*

of American Geographers, 103, 106-128.

Joseph, V. R., Hung, Y., and Sudjianto, A. (2008), "Blind kriging: A new method for developing metamodels," *Journal of mechanical design*, 130, 031102.

Fassò, A., and Cameletti, M. (2010), "A unified statistical approach for simulation, modeling, analysis and mapping of environmental data." *Simulation*, 86, 139-153.

Li, K. C., Aragon, Y., Shedden, K., and Agnan, C. T. (2003), "Dimension reduction for multivariate response data," *Journal of the American Statistical Association*, 98, 99-109.

Lue, H. H. (2009), "Sliced inverse regression for multivariate response regression," *J. Statist. Plann. Inference*, 139, 2656-2664.

Lue, H. H. (2010), "On principal Hessian directions for multivariate response regressions," *Computational Statistics*, 25, 619-632.

Lue, H. H. (2019). "Pairwise directions estimation for multivariate response regression data." *Journal of Statistical Computation and Simulation*, 89, 776-794.

Ma, P., and Kang, E. L. (2020), "A fused Gaussian process model for very large spatial data," *Journal of Computational and Graphical Statistics*, 1-11.

Martin, J. D., and Simpson, T. W. (2005), "Use of kriging models to approximate deterministic computer models," *AIAA journal*, 43, 853-863.

Thorson, J. T., Cheng, W., Hermann, A. J., Ianelli, J. N., Litzow, M. A., O'Leary, C. A., and Thompson, G. G. (2020), "Empirical orthogonal function regression: Linking population biology to spatial varying environmental conditions using climate projections," *Global Change Biology*.

Tzeng, S., and Huang, H. C. (2018), "Resolution adaptive fixed rank kriging," *Technometrics*, 60, 198-208.

Wang, W. T., and Huang, H. C. (2017). "Regularized principal component analysis for spatial data," *Journal of Computational and Graphical Statistics*, 26, 14-25.

Xia, Y., Tong, H., Li, W. K., and Zhu, L. X. (2002), "An adaptive estimation of dimension reduction space," *Journal of the Royal Statistical Society, Series B*, 64, 363-410.

Table 1. Averaged RIMSE and RPMSE for applying different methods to data generated from model in (14) and (15) in 100 replicates for high-noise cases ($c=2$) and low-noise cases ($c=10$). Values given in parentheses are the corresponding standard errors.

c		PDE	naive	spTimer	kriging	mgcv
10	RIMSE	0.610 (0.261)	6.777 (0.308)	5.542 (0.438)	0.941 (0.207)	5.334 (0.255)
	PMSE	0.155 (0.071)	1.471 (0.073)	1.090 (0.068)	0.194 (0.049)	1.032 (0.050)
2	RIMSE	1.434 (0.109)	6.073 (0.433)	5.448 (0.447)	1.593 (0.090)	1.543 (0.085)
	PMSE	0.329 (0.028)	1.451 (0.084)	1.298 (0.092)	0.372 (0.029)	0.358 (0.025)

Table 2. Averaged RIMSE and RPMSE for applying different methods to data generated from model in (14) and (16) in 100 replicates. Values given in parentheses are the corresponding standard errors.

	PDE	PDE+	naive	spTimer	kriging	mgcv
RIMSE	1.085 (0.594)	0.945 (0.527)	5.433 (1.265)	3.822 (0.992)	0.932 (0.218)	4.227 (0.882)
PMSE	0.273 (0.151)	0.238 (0.136)	1.070 (0.249)	0.921 (0.235)	0.186 (0.045)	0.856 (0.176)

Table 3. Averaged RIMSE and RPMSE for applying different methods to data generated from model in (14) and (17) in 100 replicates. Values given in parentheses are the corresponding standard errors.

	PDE	PDE+	naive	spTimer	kriging	mgcv
RIMSE	2.979 (0.350)	3.053 (0.291)	3.587 (0.688)	3.158 (0.562)	2.340 (0.226)	3.131 (0.347)
PMSE	0.677 (0.085)	0.693 (0.070)	0.837 (0.175)	0.734 (0.143)	0.551 (0.072)	0.714 (0.085)

Table 4. Averaged RIMSE and RPMSE for applying different methods to Canadian Weather data in 100 validations based on random partitions. Values given in parentheses are the corresponding standard errors.

	PDE	PDE+	naive	spTimer	kriging	mgcv
RIMSE	107.33 (24.40)	44.24 (23.54)	112.67 (32.48)	108.12 (32.89)	95.32 (31.69)	1405.61 (6269.96)
PMSE	5.821 (1.620)	2.739 (1.865)	6.676 (2.056)	6.474 (2.090)	5.799 (2.089)	145.03 (643.53)

Table 5. Averaged RIMSE and RPMSE for applying different methods to Italy Cigarette data in 100 validations based on random partitions. Values given in parentheses are the corresponding standard errors.

	PDE	PDE+	naive	spTimer	kriging	mgcv
RIMSE	6.590 (0.686)	3.461 (0.834)	3.798 (0.874)	3.746 (0.884)	3.778 (0.889)	8.064 (13.591)
PMSE	1.111 (0.129)	0.675 (0.189)	0.733 (0.201)	0.728 (0.204)	0.729 (0.201)	1.749 (4.525)

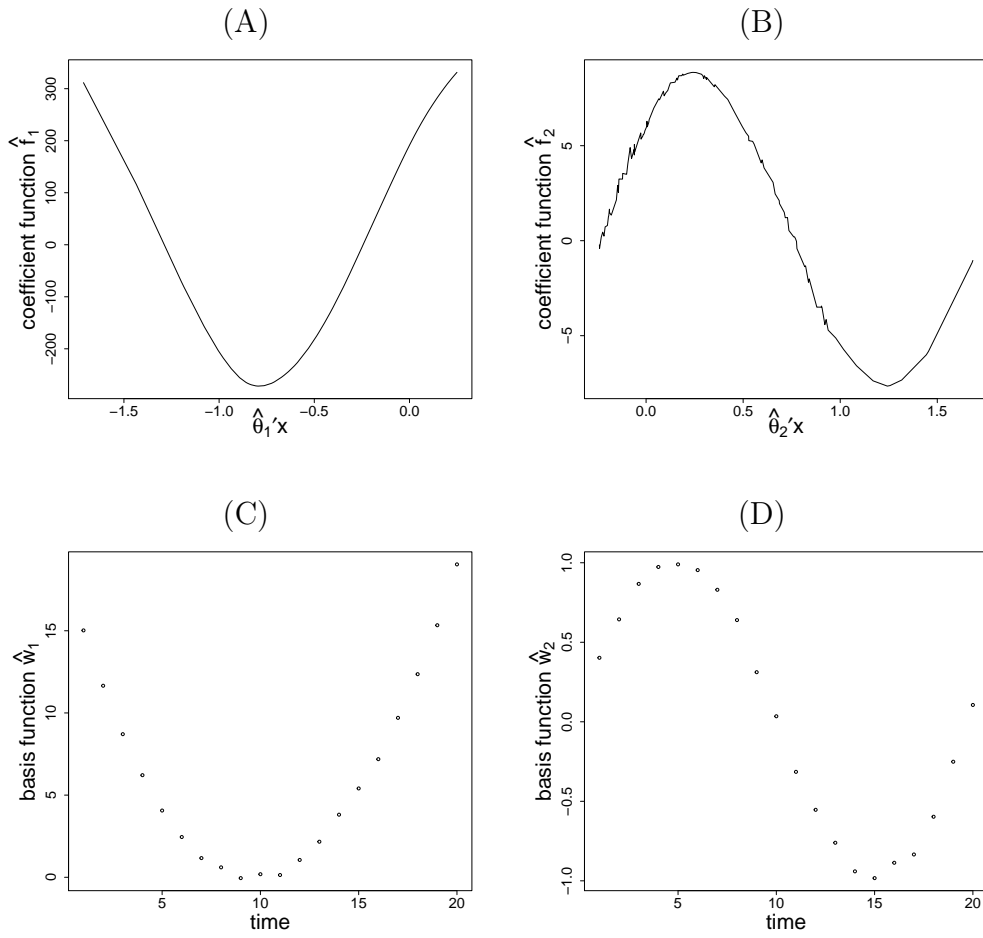


Figure 1: Plots of (A) the first and (B) the second coefficient functions with (C) the first and (D) the second basis functions for a randomly selected simulation from model in (14) and (15).

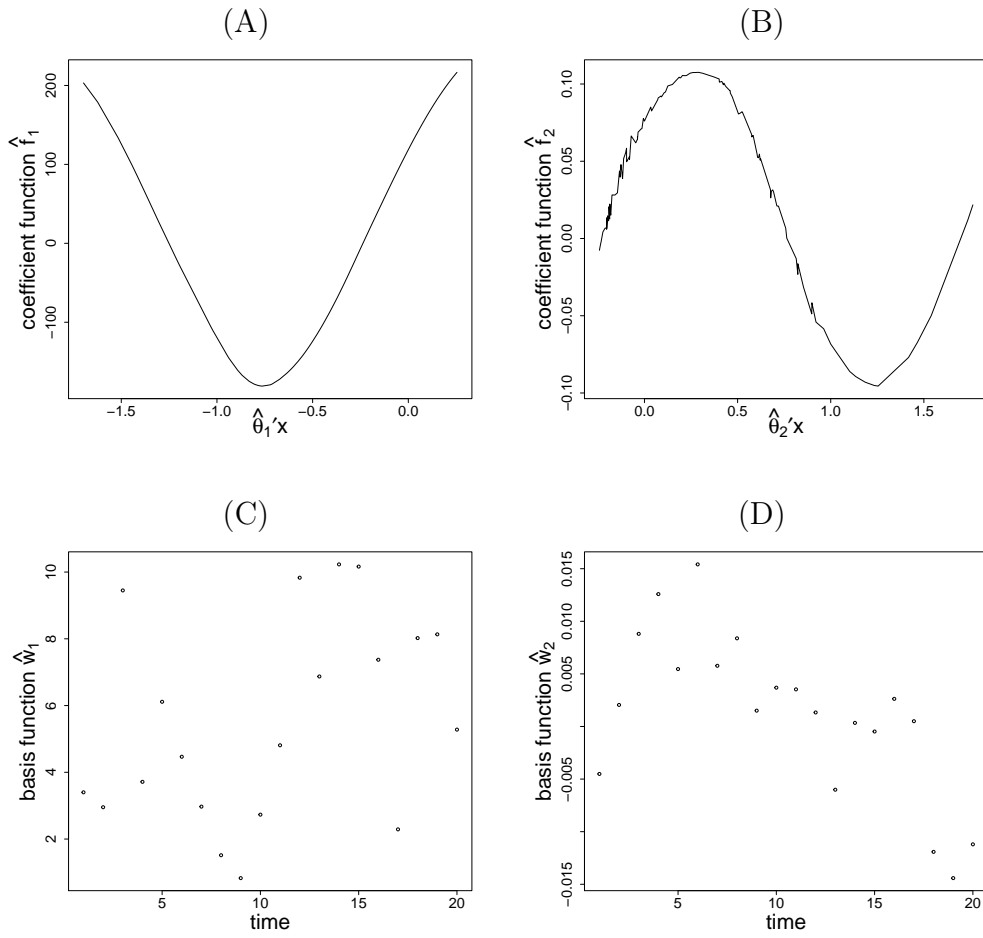


Figure 2: Plots of (A) the first and (B) the second coefficient functions with (C) the first and (D) the second basis functions for a randomly selected simulation from model in (14) and (16).

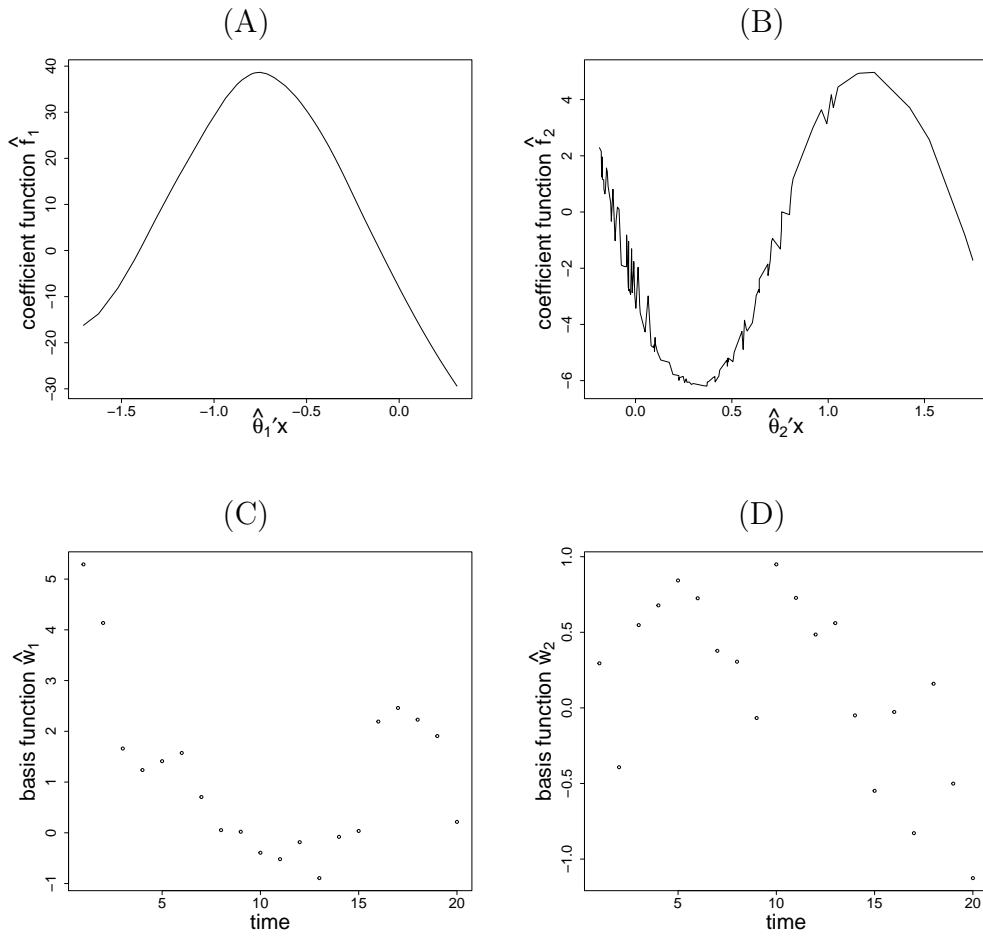


Figure 3: Plots of (A) the first and (B) the second coefficient functions with (C) the first and (D) the second basis functions for a randomly selected simulation from model in (14) and (17).

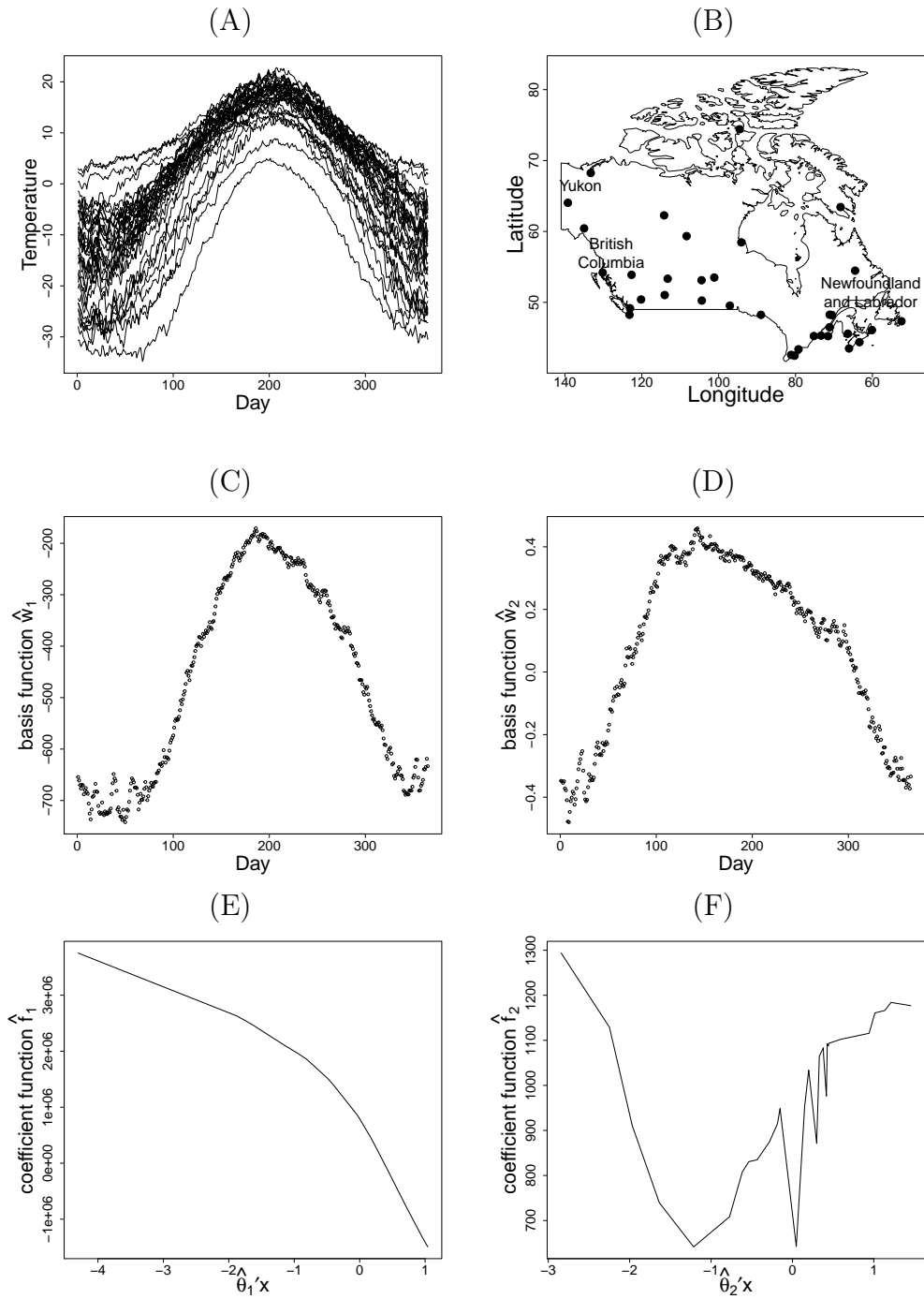


Figure 4: Plots of (A) the average daily temperatures over individual locations, (B) the spatial distribution of locations, (C) the first and (D) the second basis functions, and (E) the first and (F) the second coefficient functions for Canadian Weather data.

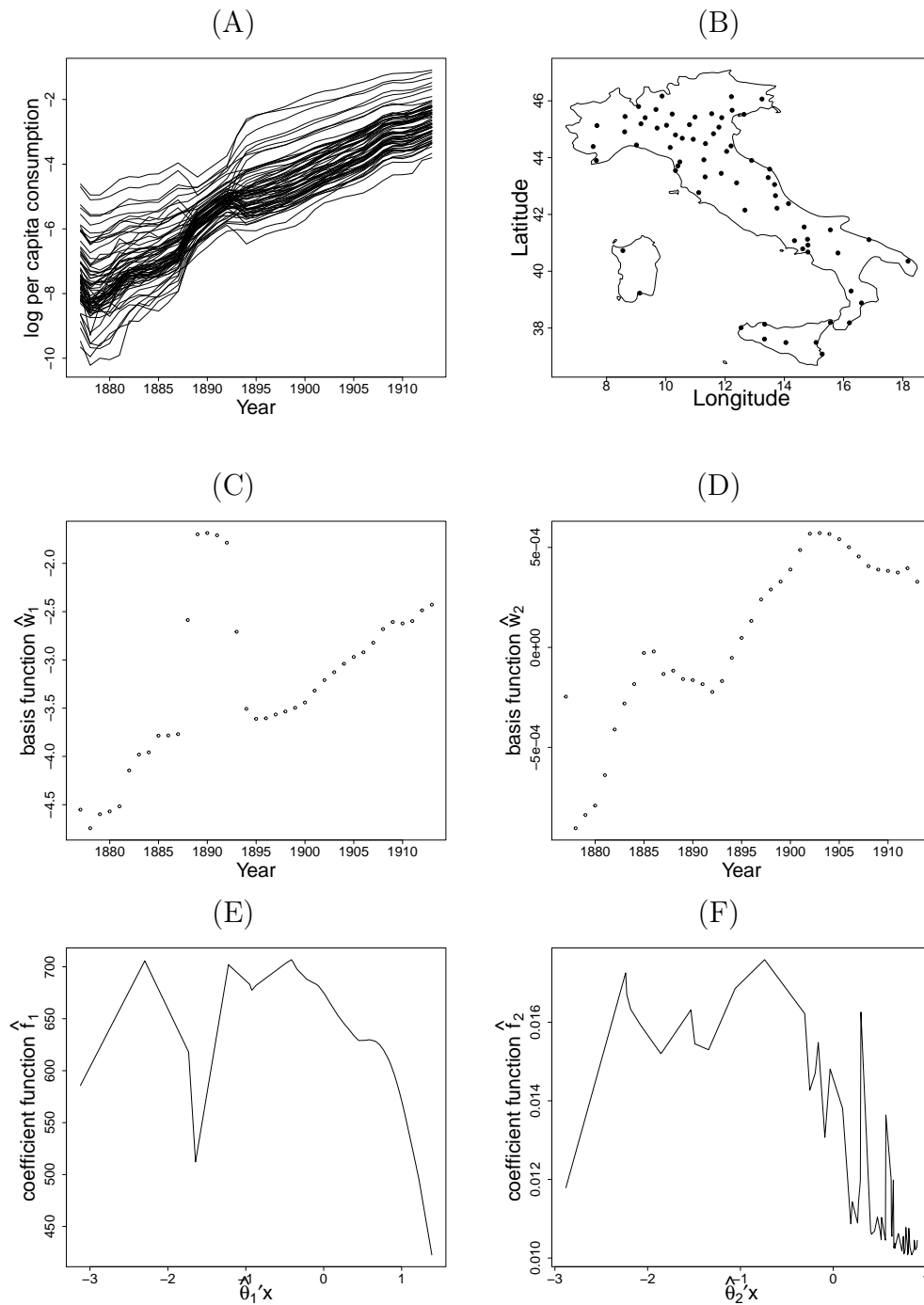


Figure 5: Plots of (A) logarithm of per capita consumption of cigarettes (kg) over individual provinces, (B) the spatial distribution of provinces, (C) the first and (D) the second basis functions, and (E) the first and (F) the second coefficient functions for Italy Cigarette data.